Band structure engineering through orbital interaction for enhanced thermoelectric power factor

Hong Zhu, Wenhao Sun, Rickard Armiento, Predrag Lazic, and Gerbrand Ceder

Citation: Appl. Phys. Lett. **104**, 082107 (2014); doi: 10.1063/1.4866861
View online: https://doi.org/10.1063/1.4866861
View Table of Contents: http://aip.scitation.org/toc/apl/104/8
Published by the American Institute of Physics

Band structure engineering through orbital interaction for enhanced thermoelectric power factor

Hong Zhu,[1] Wenhao Sun,[1] Rickard Armiento,[2] Predrag Lazic,[3] and Gerbrand Ceder[1]
[1]*Department of Materials Science and Engineering, Massachusetts Institute of Technology, 77 Massachusetts Avenue, Cambridge, Massachusetts 02139, USA*
[2]*Department of Physics, Chemistry and Biology (IFM), Linköping University, SE-58183 Linköping, Sweden*
[3]*Theoretical Physics Division, Rudjer Boskovic Institute, Bijenicka Cesta 54, Zagreb, Croatia*

(Received 12 January 2014; accepted 10 February 2014; published online 26 February 2014)

Band structure engineering for specific electronic or optical properties is essential for the further development of many important technologies including thermoelectrics, optoelectronics, and microelectronics. In this work, we report orbital interaction as a powerful tool to finetune the band structure and the transport properties of charge carriers in bulk crystalline semiconductors. The proposed mechanism of orbital interaction on band structure is demonstrated for IV-VI thermoelectric semiconductors. For IV-VI materials, we find that the convergence of multiple carrier pockets not only displays a strong correlation with the *s-p* and spin-orbit coupling but also coincides with the enhancement of power factor. Our results suggest a useful path to engineer the band structure and an enticing solid-solution design principle to enhance thermoelectric performance. © *2014 AIP Publishing LLC*. [http://dx.doi.org/10.1063/1.4866861]

Thermoelectrics are a potentially important technology for the conversion of heat flows to electrical work and vice-versa.[1] The thermoelectric figure of merit, zT, can be increased by minimizing the thermal conductivity (κ) and/or maximizing the power factor (σS^2), where σ and S are the electrical conductivity and Seebeck coefficient.[2] Over the last two decades, significant progress has been made to reduce the lattice component of thermal conductivity (κ_L) via solid-solution alloying and nanostructuring.[3–6] With κ_L approaching its amorphous limit,[7] further enhancement of zT may have to come from improvement of σS^2.[8] The optimal σS^2 is dependent on $\mu(m^*/m_e)^{3/2}$, where μ is the carrier mobility and m^* and m_e are the density-of-states effective mass and the electron rest mass.[9,10] In a single parabolic band model, this strategy requires conflicting band curvatures—flat bands will result in large m^*, but dramatically reduce μ. Recently, a strategy to address this dilemma has appeared, focusing on increasing the number of degenerate carrier pockets at the Fermi energy, since it maximizes m^* without sacrificing μ of each band.[10] This can happen when multiple bands have band extrema around the same energy (orbital degeneracy) or when multiple carrier pockets of one band in the Brillouin zone are degenerate (valley degeneracy).[11]

The success of increasing valley degeneracy for high thermoelectric performance has been demonstrated in the premier thermoelectric material, lead telluride (PbTe). PbTe is a small band gap semiconductor with two band extrema for both conduction and valence bands—the band extrema at the L point (with a multiplicity of 4 in the whole Brillouin zone) and an additional, heavier pocket along the Σ line (with a multiplicity of 12) (see Fig. 1). By alloying *p*-type PbTe with appropriate amounts of PbSe, a high valley degeneracy of 16 is obtained for the valence band due to the convergence of the L and Σ pockets. This leads to a simultaneous enhancement of S and σ, as well as a high zT value of 1.8, compared to 0.8 for pure PbTe.[10] Another example of such band engineering is the doping of Mg_2Si with Sn to increase the orbital degeneracy by aligning the two low-lying conduction bands, leading to an exceptionally large zT value of 1.3.[12] Despite the experimental success of such isostructural solid-solution alloying, the fundamental mechanisms that allow manipulation of band structures via handles, such as chemical composition, are presently not well understood. Because of this, it is unclear *a priori* whether or not a given thermoelectric material can be improved, and even if it can be, what design parameters can be used for efficient band convergence.

In this work, we report a strong correlation between the orbital interaction and particular band structure features such as band degeneracy. We find that the strength of the orbital interaction can be tuned by manipulating the interatomic distance or by chemically varying the relative positions of atomic orbitals through composition modification. Specifically, for IV-VI thermoelectric semiconductors, i.e., lead/tin/germanium chalcogenides, we find that the convergence of carrier pockets is dependent on the strength of the *s-p* orbital interaction as well as the spin-orbit coupling (SOC). Our transport calculations also demonstrate that the enhancement of power factor coincides with such a band convergence. Although this work investigates the IV-VI semiconductors as a prototype for explaining the proposed mechanism of orbital interaction on band structure, our conclusions are applicable to other systems (e.g., Sb_2Te_3 group materials with *s-p* mixing and ZnO group materials with *p-d* mixing). Our results suggest a path to engineer the band structure, i.e., towards high band degeneracy for enhanced thermoelectric properties.

Density functional theory (DFT) calculations were performed with the Perdew-Burke-Ernzerhof (PBE)[13] generalized gradient approximation (GGA) and projector augmented wave (PAW)[14] pseudopotentials, as implemented in Vienna *ab initio* simulation package (VASP).[15] For the geometry relaxation of the primitive unit cell of PbTe group materials in the rock-salt (NaCl) structure, we considered

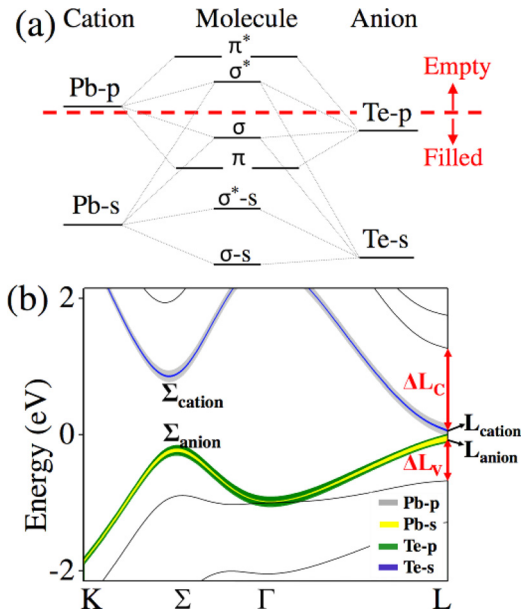

FIG. 1. Schematic of (a) MO diagram of a PbTe molecule and (b) band structure of solid state NaCl-type PbTe at the optimized lattice parameters, with the high lying valence band and low lying conduction band projected onto the Pb and Te atomic orbital makeup—the curve widths indicate the relative strengths of each contribution. The valence band maxima, namely, Σ_{anion} and L_{anion}, are mainly composed of Te-$p_{x,y}$ + Pb-s and Te-$p_{x,y,z}$ + Pb-s, respectively. The two conduction band minima, Σ_{cation} and L_{cation}, have similar characters, except that the identity of Pb and Te are interchanged. The energy difference between the two highest valence bands (or between the two lowest conduction bands) at the L point of the Brillouin zone is represented as ΔL_V (or ΔL_C).

spin-orbit coupling and applied a k-point mesh of $12 \times 12 \times 12$. The calculated equilibrium lattice parameters are in good agreement with available experiments as shown in Table I. The electronic structure used to determine the transport properties were obtained from calculations with much denser k-point meshes ($23 \times 23 \times 23$). Using the Boltzmann transport equation and constant relaxation-time approximation as implemented in the BOLTZTRAP code,[16,17] we calculated the maximum power factor relative to the relaxation time, $S^2\sigma/\tau$. Since the corresponding Fermi levels for optimal $S^2\sigma/\tau$ of holes and electrons are deep within the valence and conduction bands, respectively, further correction to E_g using a scissor operator is not considered in our transport calculations.

TABLE I. Computed lattice parameter and band gap (E_g) using PAW method with SOC compared with the available experiments.[18] E_g is defined as the energy difference between the cation-p orbital dominated states and the anion-p dominated states around the Fermi-level. A negative E_g indicates inversion of these around the gap.

	Lattice parameter (Å)		E_g (eV)		
				Expt	
System	PAW-SOC	Expt	PAW-SOC	4.2 K	300 K
PbTe	6.556	6.462	0.09	0.19	0.31
PbSe	6.182	6.124	−0.05	0.15	0.28
PbS	5.981	5.936	0.11	0.29	0.41
SnTe	6.40	6.327	−0.12	…	−0.18
SnSe	6.041	…	−0.24	…	…
SnS	5.829	5.8	−0.18	…	…
GeTe	6.012	5.985	0.23	…	…
GeSe	5.655	…	−0.06	…	…
GeS	5.428	…	−0.07	…	…

Using PbTe as an example, we now discuss the electronic structure of IV-VI semiconductors. Fig. 1(a) schematically draws the molecular orbital (MO) diagram of a PbTe molecule. Due to the s-p coupling effect, the σ bond has predominantly Te-p and Pb-s character, while σ^* mainly consists of Pb-p and Te-s. With a stronger s-p coupling, σ and σ^* bonds both move upward. We also note that due to the larger energy difference between Pb-p and Te-s orbitals compared to Te-p and Pb-s, the s-p mixing strength of the σ^* bond is smaller than that of the σ bond. Fig. 1(b) shows the relevant part of the band structure of PbTe at the optimized lattice parameter with the inclusion of SOC, which is necessary to represent the band splitting of this group of materials.[19] The band gap of PbTe is direct and occurs at the L point. The top of the valence band and the bottom of the conduction band correspond to the σ and σ^* bonds in the MO picture.[19,20] The valence band maxima at L and Σ are mainly composed of Te-$p_{x,y,z}$ + Pb-s and Te-$p_{x,y}$ + Pb-s, as represented by L_{anion} and Σ_{anion}. The two conduction band minima (CBM) (L_{cation} and Σ_{cation}) have similar characters, except that the identity of Pb and Te are interchanged (see supplementary material in Ref. 21). A high valley degeneracy of 16 in the Brillouin zone can be obtained by aligning the L and Σ carrier pockets of the conduction/valence band. Such an alignment can be characterized by the energy difference between the L and Σ valleys, namely, $(L–\Sigma)_C$ or $(L–\Sigma)_V$. In fact, the number of conducting carrier pockets can be further increased to 20 with an enhanced orbital degeneracy by converging two bands at the L point. L_{anion} and L_{cation} have symmetries of L_6^+ and L_6^-.[19] With the inclusion of SOC, the π (or π^*) bond in the MO diagram splits into two states at the L point in the band structure diagram, namely, $L_{4,5}^+$ and L_6^+ (or $L_{4,5}^-$ and L_6^-) (see Fig. 2). The orbital

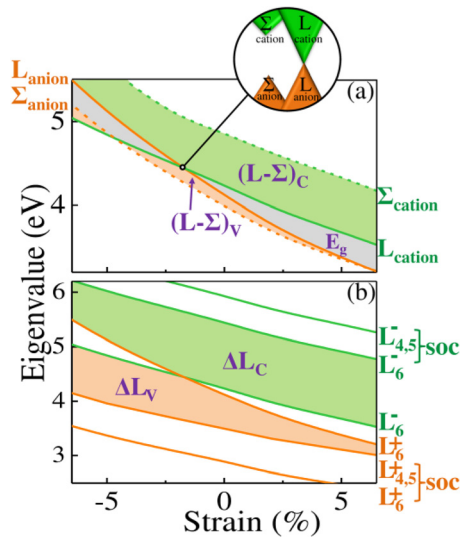

FIG. 2. Band structure variation upon hydrostatic strain: (a) eigenvalues of Σ_{anion}, L_{anion}, Σ_{cation} and L_{cation} states, and (b) eigenvalues of three highest valence states and three lowest conduction states at the L point. Valley convergence [$(L\text{-}\Sigma)_V$ and $(L\text{-}\Sigma)_C$], orbital convergence at L point (ΔL_V and ΔL_C), and E_g are indicated in the figure.

degeneracy can be characterized by the energy difference between the two highest valence bands (or between the two lowest conduction bands) at the L point, which is represented as ΔL_V (or ΔL_C) in Fig. 1.

One approach to tune the *s-p* mixing is through strain, which can result from an externally applied stress, thermal expansion, alloying/doping, or lattice mismatch in heterostructures. Here, we use PbTe as an example to demonstrate how hydrostatic strain affects the band structure by tuning the orbital interaction strength. In general, the *s-p* mixing strengths of the four band extrema in PbTe follow the trend of $L_{anion} > \Sigma_{anion} > L_{cation} > \Sigma_{cation}$, in light of different symmetries and *s-p* energy splits. But due to the fact that the two low-lying cation levels at the L point have the same symmetry of L_6^-, they tend to repel each other (see Fig. 2). This repulsion not only leads to a much larger $(L–\Sigma)_C$ than $(L–\Sigma)_V$ but also restricts the rise of L_{cation} with the increase of *s-p* coupling upon compression. The dependence of the four band extrema on strain thus follows the trend of $L_{anion} > \Sigma_{anion} > \Sigma_{cation} > L_{cation}$ (see Fig. 2(a)). Since compressive strain can raise L_{anion} above L_{cation}, the valley convergence can be described as

$$(L - \Sigma)_V = \min(L_{anion}, L_{cation}) - \Sigma_{anion}, \quad (1)$$

$$(L - \Sigma)_C = \Sigma_{cation} - \max(L_{anion}, L_{cation}). \quad (2)$$

As shown in Fig. 2(a), $(L–\Sigma)_V$ and $(L–\Sigma)_C$ of PbTe first increase with compressive strain. Once the critical strain where L_{anion} and L_{cation} cross is approached, they start to decrease with further compression.

Fig. 2(b) illustrates the orbital convergence of PbTe at the L point as a function of strain. With the increase of Te-*p* and Pb-*s* orbital coupling, the L_{anion} (the higher L_6^+) state shifts away from the lower anion L state ($L_{4,5}^+$), which results in a larger ΔL_V. In other words, extensive strain appears to increase the orbital degeneracy of holes. On the other hand, the symmetry-induced repulsion prevents L_{cation} (the lower L_6^-) state from collapsing to the next L_6^- state. Applying a compressive strain to invert the higher L_6^+ and the lower L_6^- states avoids such a repulsion and leads to a smaller ΔL_C. Thus, a high orbital degeneracy of the valence band can be achieved upon extensive strain, while for the conduction band it can be enhanced mainly upon compression.

Previously, we have demonstrated that strain could be applied to tune the valley and orbital degeneracies. Next, we discuss the feasibility of chemically shifting the relative position of the *s* and *p* atomic orbitals to adjust their coupling strengths. Table I shows the computed E_g for IV-VI semiconductors at their optimized lattice parameter. E_g is defined as the difference in energy of the states dominated by the cation *p* and anion *p* orbitals around the Fermi level. For PbTe at relaxed lattice parameter, this is the CBM and VBM, respectively. Relative to PbTe, some of the compounds (e.g., SnTe) have opposite orbital characters at the band extrema,[22] which we indicate by a negative E_g. As summarized in Fig. 3, the band degeneracies of IV-VI materials display a similar dependence on strain. More interestingly, we find that these band degeneracies have a strong correlation with the relative position of *s* and *p* orbitals of the two constituent elements (see Figs. 3 and 4). For the valence band, we find that a larger energy split between anion *p* and cation *s* orbitals ($E_{anion-p} - E_{cation-s}$) gives a higher band degeneracy (or smaller $(L–\Sigma)_V$ and ΔL_V). An example of $(L–\Sigma)_V$ as a function of $E_{anion-p} - E_{cation-s}$ for IV-VI semiconductors at a fixed lattice parameter of 6.1 Å is provided in Fig. 4(b). For the conduction band, both SOC and *s-p* coupling determine the band degeneracy. Different from the valence band, a high conduction band degeneracy can be

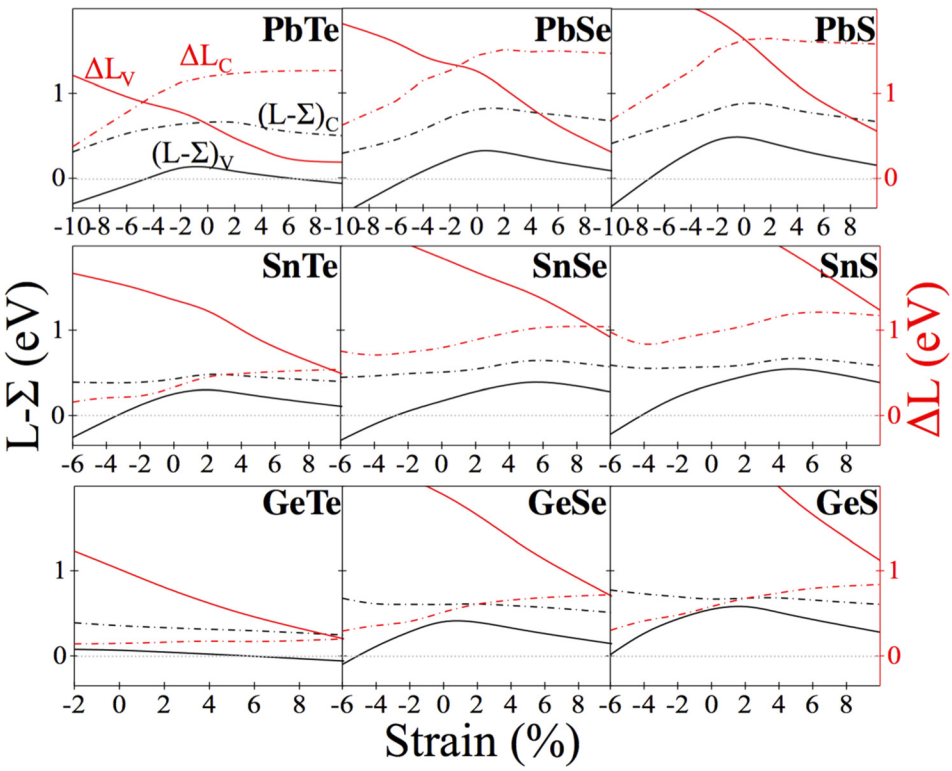

FIG. 3. Valley convergence (L–Σ) and orbital convergence (ΔL) as a function of strain for IV-VI thermoelectric semiconductors, which are shown in black and red. The solid and dashed lines represent the data for valence and conduction bands, respectively. The compressive strain is shown upto the value when E_g is zero due to the overlapping of the conduction and valence bands. See supplementary material for calculated E_g as a function of strain.[21]

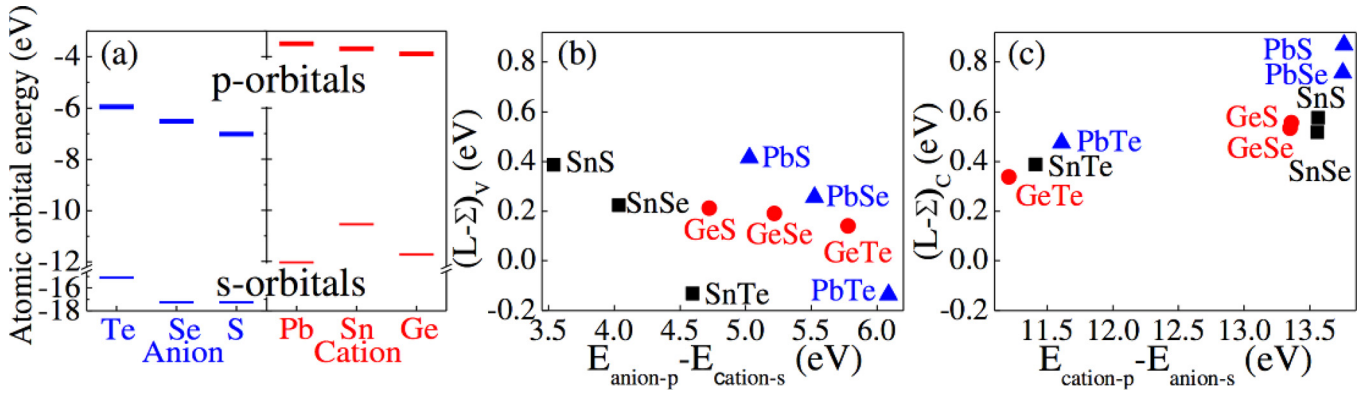

FIG. 4. (a) Atomic orbital energy (eV) of anions (Te, Se, S) and cations (Pb, Sn, Ge), (b) valley convergence of valence band, $(L–\Sigma)_V$, as a function of energy split between anion p and cation s orbitals ($E_{anion-p} - E_{cation-s}$), and (c) valley convergence of conduction band, $(L–\Sigma)_C$, as a function of energy split between cation p and anion s orbitals ($E_{cation-p} - E_{anion-s}$). The thin and thick bars represent the s and p orbitals, respectively. The lattice parameter is chosen to be 6.1 Å for (b) and (c) to identify the correlation between band convergence and energy split between atomic orbitals.

obtained with a small energy split between cation p and anion s orbital ($E_{cation-p} - E_{anion-s}$) (see Fig. 4(c) for the example of the valley convergence of conduction bands). Moreover, when we go from Pb → Ge, the SOC effect decreases significantly, which leads to a reduced repulsion of the two L_6^- states and a better convergence of conduction bands. By investigating the IV-VI group materials under different strains, we have noticed that: (1) the valence band extrema can be converged by increasing $E_{anion-p} - E_{cation-s}$; (2) a high conduction band degeneracy can be achieved with a reduced $E_{cation-p} - E_{anion-s}$ and/or a smaller SOC of cations.

We next investigate the optimal power factor ($S^2\sigma/\tau$). Here, we focus on the results of lead chalcogenides (see Fig. 5). Tin and germanium chalcogenides present similar results and hence are not shown here. When we go from PbTe to PbS, the optimal $S^2\sigma/\tau$ decreases for both holes and electrons, which can be attributed to the better band convergence of PbTe. For holes, we find that the optimal power factor is strongly correlated to the band convergence. This correlation is most notorious in PbSe and PbS, while in the case of PbTe, the L and Σ valleys of valence bands are close enough to be effectively converged at high temperatures, due to the broadening of the Fermi distribution.[10] In light of the strong SOC effect of Pb, a large power factor of electrons can be only achieved upon a compressive strain when there is no repulsion between CBM and the higher L_6^- state. On the other hand, Ge- and Sn-based chalcogenides with smaller SOC in the cations present higher n-type $S^2\sigma/\tau$, due to the enhanced conduction band degeneracy.

We are thus led to conclude that s-p orbital interaction and spin-orbit coupling can be used to engineer the band structure and the transport properties of IV-VI semiconductors. Such a tunability of band structure with orbital interaction should maintain its generality in other materials with similar interactions, but the quantitative correlation may need further investigation in each group of materials. For example, the band gap of II-VI semiconductors varies with the p-d repulsion of the VBM. Compared to ZnTe and CdTe, HgTe with a smaller energy split between the cation d and anion p orbitals shows a stronger orbital repulsion and hence a smaller band gap.[23] Similar to alloying and quantum confinement,[24,25] orbital interaction may serve as a powerful tool to fine-tune the electronic structure of a material in different application areas such as thermoelectrics, optoelectronics, and microelectronics.

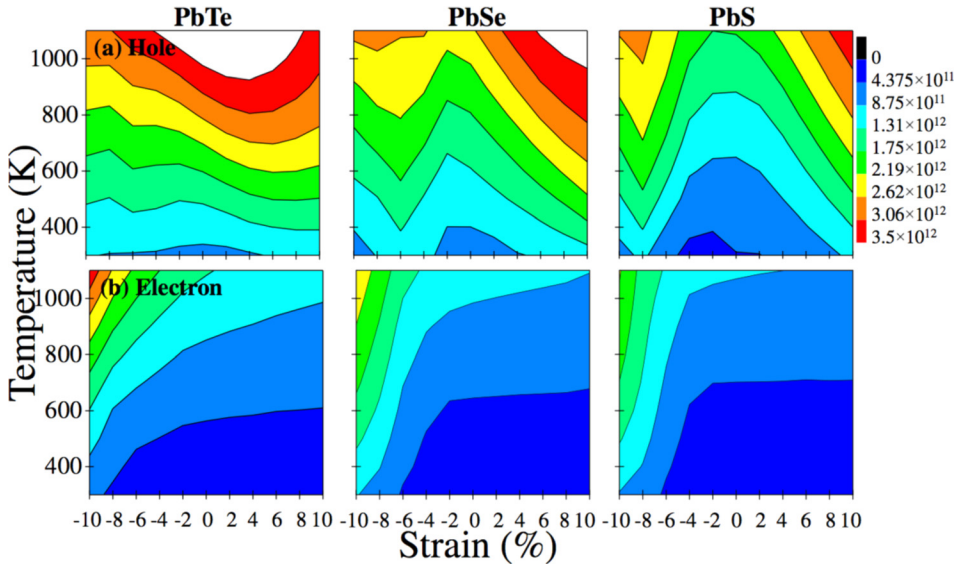

FIG. 5. The optimal power factor ($S^2\sigma/\tau$ in the unit of W/m K^2 s), of lead chalcogenides for (a) holes and (b) electrons as a function of strain (%) and temperature (K). The color scale is indicated in the figure.

The results and insights demonstrated how alloying can be used to modify the band structure in a well determined way with the objective of enhancing the band degeneracy and power factor of semiconductors. We note from Fig. 3 that both compressive and extensive strains can enhance the valence band degeneracy. Thus, one may want to alloy a *p*-type IV-VI semiconductor so as to lead to a better band convergence. For example, the valence band degeneracy of PbSe can be enhanced through PbTe alloying. However, sometimes we may have an "over-converged" band structure with $L\text{-}\Sigma < 0$. In that case, the reverse action should be taken to bring $L\text{-}\Sigma$ back to zero. It has been reported that $(L\text{-}\Sigma)_V$ of PbTe decreases as temperature increases due to thermal expansion. At 850 K, PbTe displays a negative $(L\text{-}\Sigma)_V$.[10] Alloying PbTe with 15% PbSe realigns the L and Σ carrier pockets of valence bands at such a high temperature and leads to a large *zT* of 1.8. Such a recovery of $(L\text{-}\Sigma)_V$ from negative to zero could be understood as follows: first, PbSe has a larger $(L\text{-}\Sigma)_V$ compared to PbTe; second, the inclusion of PbSe with smaller lattice parameter introduces a negative strain into $PbTe_{1-x}Se_x$, which compensates its thermal expansion. For electrons, the introduction of compressive strains and cations with small SOC appears to be efficient at converging the conduction band extrema. Thus, a preferred alloy phase for *n*-type IV-VI materials shall possess smaller lattice parameter or SOC in cations. For example, $Pb_{1-x}Ge_xTe$ is likely to be good *n*-type thermoelectric materials. In fact, it has been reported that 5% GeTe inclusion into PbTe was able to increase the *zT* from 0.8 to ~1.3.[26]

In summary, we have explained recent experimental advances in increased power factor for thermoelectric materials in terms of orbital interactions. Our results suggest a general strategy for engineering band convergence by strain and composition modification. For IV-VI thermoelectric materials, we found that holes and electrons behave differently with these modifications due to the repulsion within the conduction bands. For holes, one can either apply appropriate compressive/extensive strain or split the anion *p* and cation *s* orbitals to converge the valence bands for enhanced power factors. For electrons, a higher band degeneracy may be achieved with small-SOC cations or upon compressive strains which lift L_{anion} over L_{cation} and hence eliminate the symmetry-induced repulsion within the conduction bands. Finally, we have proposed an alloying strategy to optimize the available IV-VI thermoelectric materials, which has been validated by prior experiments in some cases.

This work was supported by the Office of Naval Research under Contract No. N00014-11-1-0212. R.A. acknowledges support from the Swedish Research Council (VR), Grant No. 621-2011-4249 and the Linnaeus Environment at Linköping on Nanoscale Functional Materials (LiLi-NFM) funded by VR. We would also like to thank Professor Jeff Snyder and Vidvuds Ozolins for helpful discussions.

[1]L. E. Bell, Science **321**, 1457 (2008).
[2]J. R. Sootsman, D. Y. Chung, and M. G. Kanatzidis, Angew. Chem., Int. Ed. **48**, 8616 (2009).
[3]B. Poudel, Q. Hao, Y. Ma, Y. Lan, A. Minnich, B. Yu, X. Yan, D. Wang, A. Muto, D. Vashaee *et al.*, Science **320**, 634 (2008).
[4]J. Tang, H. Wang, D. H. Lee, M. Fardy, Z. Huo, T. Russell, and P. Yang, Nano Lett. **10**, 4279 (2010).
[5]J. Yu, S. Mitrovic, D. Tham, J. Varghese, and J. R. Heath, Nat. Nanotechnol. **5**, 718 (2010).
[6]K. Biswas, J. He, I. D. Blum, C. Wu, T. P. Hogan, D. N. Seidman, V. P. Dravid, and M. G. Kanatzidis, Nature **489**, 414 (2012).
[7]C. J. Vineis, A. Shakouri, A. Majumdar, and M. G. Kanatzidis, Adv. Mater. **22**, 3970 (2010).
[8]J. P. Heremans, V. Jovovic, E. S. Toberer, A. Saramat, K. Kurosaki, A. Charoenphakdee, S. Yamanaka, and G. J. Snyder, Science **321**, 554 (2008).
[9]H. J. Goldsmid, J. Electron. Mater. **42**, 1482 (2013).
[10]Y. Pei, X. Shi, A. LaLonde, H. Wang, L. Chen, and G. J. Snyder, Nature **473**, 66 (2011).
[11]Y. Pei, H. Wang, and G. J. Snyder, Adv. Mater. **24**, 6125 (2012).
[12]W. Liu, X. Tan, K. Yin, H. Liu, X. Tang, J. Shi, Q. Zhang, and C. Uher, Phys. Rev. Lett. **108**, 166601 (2012).
[13]J. P. Perdew, K. Burke, and M. Ernzerhof, Phys. Rev. Lett. **77**, 3865 (1996); **78**, 1396 (1997).
[14]P. E. Blöchl, Phys. Rev. B **50**, 17953 (1994).
[15]G. Kresse and J. Furthmuller, Phys. Rev. B **54**, 11169 (1996).
[16]G. K. H. Madsen, J. Am. Chem. Soc. **128**, 12140 (2006).
[17]G. K. H. Madsen and D. J. Singh, Comput. Phys. Commun. **175**, 67 (2006).
[18]*Semiconductors: Group IV Elements, IV-IV and III-IV Compounds*, Landolt-Börnstein, New Series, Group III, Vol. 41, Part A, edited by O. Madelung, U. Rossler, and M. Schulz (Springer-Verlag, Berlin, 2005); B. F. Bilenkii, A. G. Mikolaichuk, and D. M. Freik, Phys. Status Solidi **28**, K5 (1968); T. Chattopadhyay, J. X. Boucherle, and H. G. vonSchnering, J. Phys. C: Solid State Phys. **20**, 1431 (1987).
[19]S.-H. Wei and A. Zunger, Phys. Rev. B **55**, 13605 (1997).
[20]H. Peng, J. Song, M. G. Kanatzidis, and A. J. Freeman, Phys. Rev. B **84**, 125207 (2011).
[21]See supplementary material at http://dx.doi.org/10.1063/1.4866861 for orbital projected band structure of PbTe at relaxed lattice parameter and the computed E_g for lead, tin, and germanium chalcogenides as a function of hydrostatic strain.
[22]T. H. Hsieh, H. Lin, J. Liu, W. Duan, A. Bansil, and L. Fu, Nat. Commun. **3**, 982 (2012).
[23]S.-H. Wei and A. Zunger, Phys. Rev. B **37**, 8958 (1988).
[24]I. Vurgaftman and J. R. Meyer, J. Appl. Phys. **94**, 3675 (2003).
[25]L. D. Hicks and M. S. Dresselhaus, Phys. Rev. B **47**, 12727 (1993).
[26]I. Kudman, Metal. Trans. **2**, 163 (1971).